CHALMERS
UNIVERSITY OF TECHNOLOGY

Dynamics of large-scale bubbling fluidized bed combustion plants for heat and power production

Downloaded from: https://research.chalmers.se, 2024-07-27 08:20 UTC

Citation for the original published paper (version of record):
Martinez Castilla, G., Mocholí Montañés, R., Pallarès, D. et al (2023). Dynamics of large-scale bubbling fluidized bed combustion plants for heat and power production. Fuel, 341.
http://dx.doi.org/10.1016/j.fuel.2023.127748

N.B. When citing this work, cite the original published paper.

research.chalmers.se offers the possibility of retrieving research publications produced at Chalmers University of Technology.
It covers all kind of research output: articles, dissertations, conference papers, reports etc. since 2004.
research.chalmers.se is administrated and maintained by Chalmers Library

(article starts on next page)

Fuel 341 (2023) 127748

Contents lists available at ScienceDirect

Fuel

journal homepage: www.elsevier.com/locate/fuel

Dynamics of large-scale bubbling fluidized bed combustion plants for heat and power production

Guillermo Martinez Castilla [a,*], Rubén M. Montañés [b], David Pallarès [a], Filip Johnsson [a]

[a] Chalmers University of Technology, Hörsalsvägen 7b, Gothenburg, Sweden
[b] SINTEF Energy Research, Sem Saelandsvei 11, Trondheim, Norway

ARTICLE INFO

Keywords:
Dynamic modeling
Transient operation
Bubbling fluidized bed
Combined heat and power
Operational flexibility
Biomass combustion

ABSTRACT

Bubbling fluidized bed combustion (BFBC) plants for combined heat and power (CHP) production have traditionally been dispatched under slow load changes. As the amount of variable renewable electricity increases in energy systems worldwide, knowledge regarding the transient capabilities of the gas and water-steam sides of BFBC plants is required. The aim of this work is to investigate the dynamic performance of large-scale BFBC plants when accounting for both the gas and water-steam sides. To do so, this paper presents a dynamic model of BFB-CHP plants that result from connecting a model of the gas side to a process model of the water-steam side. The plant model output is validated by comparisons with operational data measured in a 130-MW_{th} BFBC plant that produces electricity, district heating (DH) water and steam for industrial clients. The validation shows that the model can satisfactorily describe both multi-load steady-state operation and load transients. The simulation results highlight the fact that the water-steam cycle achieves stabilization more rapidly after changes in the DH line and steam delivered to customers, as compared to changes in the combustor load. The timescales of the plant outputs for different changes have been calculated, with stabilization times ranging from 2 to 15 min for the power production versus 2–25 min characterizing the DH production. Compared to the stabilization times of the gas side, the water-steam side is an order of magnitude slower, thereby limiting the transient operation capabilities of BFB-CHP plants.

1. Introduction

The decarbonization of the power sector is considered a crucial mechanism for maintaining global warming within the target of 2 °C above pre-industrial levels [1] and relies heavily on increasing the share of energy generated from variable renewable electricity (VRE) sources [2]. The rapid increase in the penetration of non-dispatchable electricity generation brings up serious challenges with respect to power grid stability, due to the intermittent nature of VRE sources, especially when nuclear power plants are being phased-out in many energy systems worldwide [3]. As a consequence, dispatchable thermal power plants have become crucial actors when it comes to compensating for the fluctuations in power generation from VRE sources. In other words, thermal power plants will need to have their production and operational profiles adapted to the new requirements that characterize energy markets with a high penetration of VRE.

From the perspective of net-zero carbon emissions, fluidized bed combustors (FBCs) are especially attractive within the different thermal power plant technologies, due to their abilities to run efficiently solely on renewable fuel of relatively low cost (often, biomass and renewable waste fractions [4]). Among the portfolio of renewable-based FBC units, bubbling fluidized bed (BFB) combustors (BFBCs) are the preferred option owing to their lower capital costs, as compared to circulating (CFB) units at lower thermal sizes, i.e., within the 30–150 MW_{th} range, which are typical of biomass-fired boilers [5] due to the low energy density of biomass and the correspondingly high specific transport costs. Since regions in which biomass is readily available are often characterized by a large heat demand (e.g., Nordic countries, Canada, northern China), and given the combustion characteristics of biomass fuels, BFBC units are often deployed as combined heat and power (CHP) plants. Usually, in biomass-based BFB-CHP plants, the production of heat in the form of hot water for district heating (DH) or steam for industrial users governs the dispatchability of the plant [6]. Given that the demand for heat is often constant (industry-based demand) or characterized by very slow changes (weather-based demand), traditional operation of BFBC plants has been characterized by slow load changes, as compared to other combustion facilities. Thus, if BFBC plants are expected to play a

* Corresponding author.
E-mail address: castilla@chalmers.se (G. Martinez Castilla).

https://doi.org/10.1016/j.fuel.2023.127748
Received 31 October 2022; Received in revised form 10 January 2023; Accepted 22 January 2023
Available online 16 February 2023
0016-2361/© 2023 The Author(s). Published by Elsevier Ltd. This is an open access article under the CC BY license (http://creativecommons.org/licenses/by/4.0/).

Nomenclature

Greek

α	heat transfer coefficient
β	Baumann factor
ε	emissivity
η	efficiency
θ	valve opening
λ	thermal conductivity
ρ	density
ψ	enhancement factor

Latin

A	area
AP	absolute percentage error
Bo	boiling number
C	pre-exponential factor, valve flow coefficient
c	heat capacity
Co	Convection number
d	diameter
dp	pressure drop
E	total energy
F	flow rate
G	mass flow density
h	specific enthalpy
K	flow area coefficient, friction loss coefficient
k	absorption coefficient
L	length
LF	length factor
m	mass flow through a pipe, total mass
n	number
Nu	Nusselt number
P	power, pressure
Pr	Prandtl number
p	pressure
Q	heat flow
R	resistance
RC	relative change
s	thickness
T	temperature
t	time
x	variable, steam quality
y	variable

Subscripts

a	arrangement
c	condensate
comb	combustion
crit	critical point
el	electrical
f	fuel, friction
fw	feed water
g	gas
hyd	hydraulic
is	isentropic
Liq	liquid
LM	logarithmic mean
m	measured
mech	mechanical
n	element
nom	nominal
p	constant pressure, optical path
s	simulated, steam
t	turbine
tp	two-phase
v	vapor, valve
vap	vaporization
vol	volume
w	wall
0	initial, reference
∞	final

Abbreviations

BFB	bubbling fluidized bed
BFBC	bubbling fluidized bed combustor
CFB	circulating fluidized bed
CHP	combined heat and power
DH	district heating
ECO	economizer
HHV	high heating value
HP	high-pressure
HPT	high-pressure turbine
FB	fluidized bed
FBC	fluidized bed combustion
FG	flue gas
FWH	feed water heater
LPT	low-pressure turbine
OFWH	open feed water heater
RC	recirculated
SH	superheater
STC	steam to customers
VRE	variable renewable electricity

role in ensuring the flexibility of the upcoming energy systems, there is a need to investigate the transient operational capabilities of BFBC units. Exploring the limits of transient operation of BFBC plants would facilitate: the design of plants with faster responses; the retrofitting of existing facilities; and the design of control strategies that would enable the production of heat and power at the required rates and flexibility levels. Furthermore, industrial processes that consume steam are expected to be electrified in the upcoming years [7]. Therefore, the operation of these processes is expected to be adapted to follow electricity prices, entailing an additional source of variations that will need to be handled by BFB-CHP plants.

Among the different tools for investigating power plant flexibility, dynamic process modeling is attracting attention due to its general formulation approach and relatively low computational cost (as opposed to unaffordable computational fluid dynamics simulations at plant level). In particular for FBC plants, dynamic process models can include a representation of the gas side (i.e., in-furnace or reactive side) by making use of low-order, semi-empirical models that can describe a wide range of fluidized bed designs and operations [8,9]. Combining in-furnace modeling with a description of the water-steam side enables examination of the interactions between the two sides. This allows for computation of the representative time constants of different process variables, providing insights into the bottlenecks, delays, and instabilities of the process, among other factors. The need for additional research work on dynamic modeling of renewable fuel power plants has recently been highlighted by Atsonios et al. [10], who emphasized the scarcity of these types of assessments in the published literature, as compared to studies of fossil fuel plants or steady-state investigations.

When it comes to modeling the dynamics of BFBC plants, it is important to distinguish between the gas and water-steam sides. Focusing on the gas side, the work conducted by Selçuk et al. [11] stands out, in that a detailed dynamic model was presented and validated

against steady-state and transient operational data obtained from a 0.3–MW unit. The model was subsequently used to find out inverse responses of the char inventory of the dense bed after a load change. More recently, Yasar et al. [12] have presented a transient model of BFBC units coupled to a 3-D radiation model, which was validated against a lignite-fired 0.3-MW unit. Kataja et al. [13] presented the formulation of 1-D model of the furnace that was connected to a model of the steam drum and evaporator. That work also included a simulation study of the boiler responses after step changes were applied to the fuel flow. Lastly, it is worth mentioning the work of Galgano et al. [14], whose study uncovered substantial differences between the dynamic behaviors of the dense bed and freeboard regions. Martinez Castilla et al. [8] have recently published a 1.5-D dynamic model of the gas side of large-scale BFBC units, which was used to compute the inherent dynamics of the furnace. The study revealed characteristic times in the order of 1–15 min, with large differences between the bottom and top regions of the combustor. The authors carried out further investigations on the impacts of different in-furnace mechanisms on the stabilization times [9]. Regarding the water-steam side, it is worth mentioning the recent study of Zlatkovij et al. [15], in which a 0-D dynamic model of a BFB furnace was integrated into a simplified model of the water side. The model was used to test and compare different model predictive control strategies. In summary, the studies available in literature have either focused on the gas side or on the water-steam side. There is a knowledge gap regarding the overall transient behavior of BFBC plants, and there is a need for assessments of the dynamics at the plant level, i.e., accounting for the interactions of both the gas and water-steam sides. Furthermore, the models mentioned above lack validation with operational data from large-scale facilities.

This work aims at acquiring insights into the open-loop transient behaviour of large-scale BFBC plants when accounting for both the gas and water-steam sides. This is tackled by developing a dynamic model of large-scale BFBC plants that results from the integration of a process model of the water-steam side with an existing model of the gas side by the authors (a low-order semiempirical model that can describe a wide range of fluidized bed designs and operations at low computational cost) previously validated [8]. The complete plant model developed in this work is initially validated against operational data from a 130-MW_{th} reference plant, and is subsequently used to conduct a dynamic analysis of the reference plant.

2. Method

A schematic overview of the methodology and workflow followed in this study is shown in Fig. 1. With the aim of computing the transient performance characteristics of BFBC plants, a dynamic model of the gas side of BFBC units, previously presented and validated by the authors [8], is in this work connected to a model of the water-steam side, together conforming a BFB-CHP plant model (see Section 3). The BFB-CHP model is parametrized and initialized with design equipment data obtained from an industrial-size reference plant (described in Section 2.1). The reference data include the regulatory and supervisory layers of the control system. The validation of the dynamic model with steady-state and transient operational data measured in the reference plant is presented in Section 4.1. Lastly, the validated model is here used to study the reference BFB-CHP plant using a dynamic analysis, the methodology for which is presented in Section 2.2, with the related results and discussion in Section 4.2.

3. Reference plant description

The present work utilizes as reference for the construction, calibration and validation of the model an industrial BFB-CHP plant located in Örnsköldsvik, Sweden. A schematic of the plant input/output energy mix is shown in Fig. 2. The 130-MW_{th} biomass-fired plant delivers medium-pressure steam to industrial facilities, i.e., steam to customers (STC), power to the grid and DH to the nearby municipality. Table 1 summarizes the main plant characteristics and design values.

Fig. 3 shows a process schematic of the reference plant, along with the main process variables used in this work. The BFB furnace has secondary and tertiary air injection points and uses flue gas recirculation from the bottom of the furnace for bed temperature control. The internal

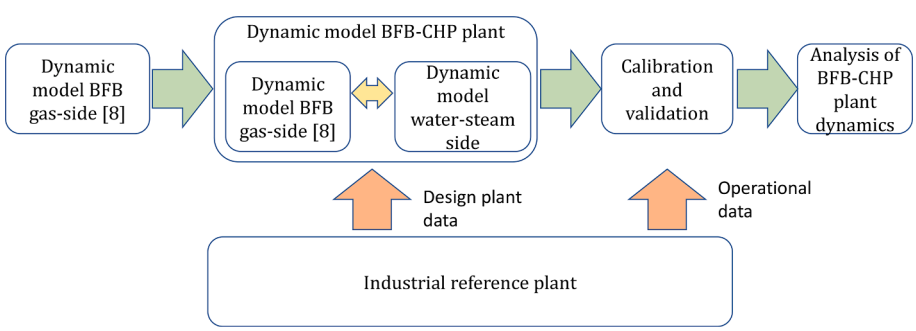

Fig. 1. Schematic overview of the methodology followed in this work.

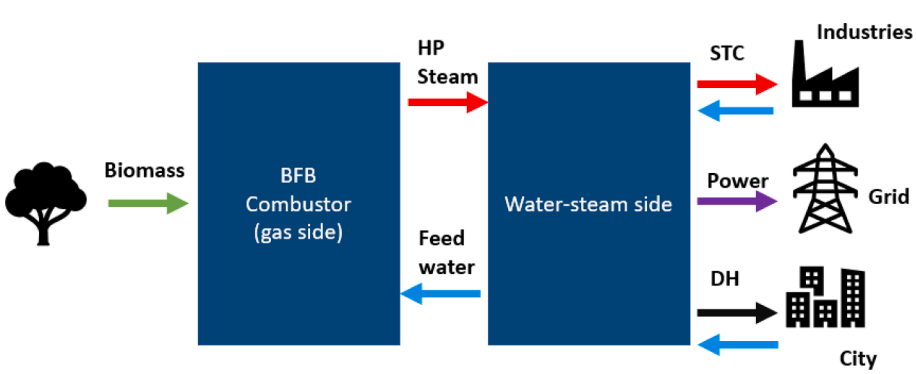

Fig. 2. Input/output scheme of the reference plant. HP, High-pressure; DH, district heating; STC, steam to customers.

Table 1
Reference plant design values.

Fuel type	Wood chips and forest residues
Furnace dimensions [m]	9.18 × 8.67 × 30
Combustor thermal load [MW_{th}]	130
Drum pressure [bar]	151.5
Live steam temperature [C]	540
Live steam flow [kg/s]	53.4
Power production [MW_{el}]	37
District heating production [MW]	60

walls of the furnace are membrane walls in which saturated water is evaporated while it naturally circulates from/to the drum. Several superheater (SH) tube bundles are vertically immersed in the wingwall of the freeboard (upper furnace). The remainder of the superheaters and economizers (ECO) are located across the flue gas flow in the convection path. Three spray attemperators (desuperheaters, DSHs) are situated within each superheating stage for steam temperature control. The steam turbine train consists of six stages, which are distributed within the high-pressure train (HPT) and the low-pressure train (LPT). Steam from the third HPT outlet is extracted and delivered as STC, while the two low-pressure condensers are used for DH production (DHCs). The feedwater is preheated prior to the economizers using three closed feedwater heaters (FWHs) and a deaerator (OFWH), whereby the make-up water and condensate returned by the industrial customers are returned into the cycle.

The conventional operation of the plant is governed by the STC demand, being the generation of DH and power the secondary and tertiary products, respectively. Thus, based on the plant layout shown in Fig. 2, a given combustor load can lead to a wide range of output mixes (referred to hereinafter as 'load levels'), depending on the STC and DH demands. In this work, two load levels of relevance for the reference plant are studied, the operational conditions for which are shown in Table 2. The selected load levels are used for steady-state validation of the plant model (see Section 4.1), as well as for initial steady-state operation prior to the dynamic analysis (see Section 4.2). Note that the load levels used in this work have very similar STC demands and differ mostly in generation of power and DH.

3.1. Dynamic analysis

The transient performance of the investigated BFB-CHP plant is assessed through so-called open-loop tests [8,9]. By disconnecting the supervisory control loops (i.e., the control loops governing the plant production levels; see Section 3.2) and introducing step-changes in the relevant inputs, the tests allow the computation of the inherent process dynamics for a given perturbation/change ensuring the effect of control loops are minimized. The list of input variables that are changed in the present work is shown in Table 3, and includes the load level at which the plant is running when the changes are introduced, as well as the magnitudes of the changes. Note that during each input variable change, the remainder of the inputs remain constant, with their values corresponding to Load level 2. It should also be noted that although the STC is an output of the plant, the choice of mass flow to be delivered is an input to the model. After the step-changes are applied, the open-loop responses of the main process variables of the water-steam side (listed in Table 4) are tracked and measured through the stabilization time t_s.

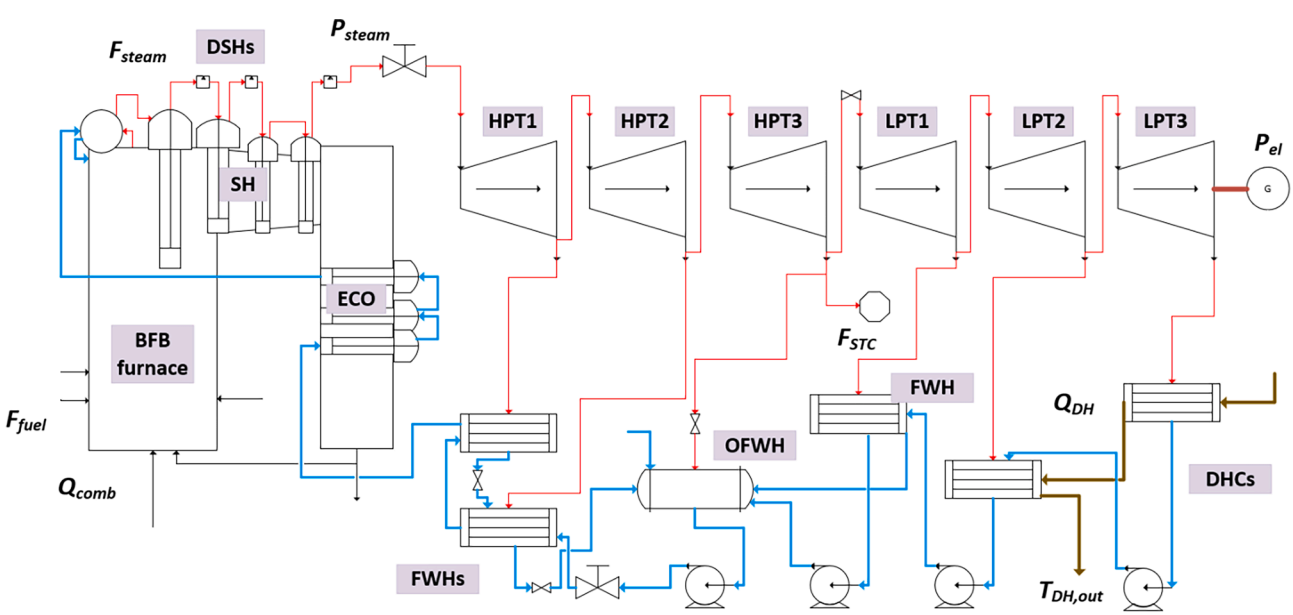

Fig. 3. Process schematic of the reference plant including the main process variables used throughout the work. Red is used for steam lines and water for water lines. SH, superheater; DSH, desuperheater; ECO, economizer; HPT, high-pressure turbine; LPT, low-pressure turbine; DHC, district heating condenser; OFWH, open feedwater heater; FWH, feedwater heater. (For interpretation of the references to colour in this figure legend, the reader is referred to the web version of this article.)

Table 2
Plant load levels (i.e., output mix) used for steady-state validation of the model.

Process variable	Load level 1 – High Power, High DH, medium STC	Load level 2 – Medium Power, Medium DH, medium STC
Fuel flow, F_{fuel} [kg/s]	14.0	8.4
Live steam flow, F_{steam} [kg/s]	53.4	29.5
STC mass flow, F_{STC} [kg/s]	13.4	15.8
Power generation, P_{el} [MW]	36.0	16.5
DH production, Q_{DH} [MW]	49.2	31.8

Table 3
Step input changes introduced in the open-loop tests.

Input variable	Relative change	Absolute change	Initial plant steady-state
Combustion load, Q_{comb} [kg/s]	−20 %	8.4 → 6.7	Load level 2
STC flow, F_{STC} [kg/s]	−20 %	15.8 → 12.6	Load level 2
DH water inflow, F_{DH} [kg/s]	−20 %	135 → 108	Load level 2

Table 4
Selected process variables used to characterize the process dynamics of the plant.

Tracked process variables	Unit
Power production, P_{el}	MW
District heating production in turbine condensers, Q_{DH}	MW
Live steam flow, F_{steam}	kg/s
Live steam pressure, P_{steam}	bar
District heating outflow temperature, $T_{DH,out}$	°C

Here, the stabilization time is defined as the time that it takes for a certain process variable to execute 90 % of the total change, i.e., when the process variable y lies within the interval defined by Equation (1). To facilitate the assessment of the interactions between plant inputs and outputs, the relative change (RC) before and after the change is also computed using Equation (2).

$$y_\infty - 0.1\Delta y < y < y_\infty + 0.1\Delta y \tag{1}$$

$$RC = 100 \bullet \frac{y_\infty - y_0}{y_0} \tag{2}$$

4. Model description

The dynamic model of BFB-CHP plants used in this work results from connecting a dynamic model of the gas side of FB boilers previously published and validated by the authors [8], with a dynamic process model of the water-steam side. The model is developed in Modelica [16].

Fig. 4 shows a simplified diagram of the plant model, including a simplified representation of the main mass and energy streams. Inputs to the model include: geometric data of the furnace and process equipment; the properties of the fuel and bulk solids; the incoming DH water temperature and flow; and the plant operating load (i.e., desired output production). The following subsections describe the two parts (gas side and water-steam side) of the BFB-CHP plant model.

4.1. BFB gas side

The combustor side is described by a number of perfectly mixed control volumes exchanging mass and energy. In the BFB mode, the model domain is divided into two fluid-dynamic regions, the dense bed and the freeboard, each of which is described as a consecution of N control volumes (represented by B and F, respectively, in Fig. 4). Three phases are included in the model: bulk solids (modeled as a mean size); gas (as an ideal gas mixture of nine components); and fuel (modeled as fresh, dry, and devolatilized in order to account for the changes in size and density as fuel conversion evolves). All of the solid phase is assumed to remain in the bottom region, i.e., neglecting the entrainment of solids. Radiation is assumed to be the dominant mechanism for bed-wall heat transfer in the freeboard, and as such, convective heat transfer to the waterwalls is neglected. This assumption is traditionally considered valid when designing and modeling BFB furnaces (see [17;18]) and based on the relatively low gas velocity throughout the riser under bubbling fluidized bed conditions (<1.5 m/s), which yields solids concentration values in the freeboard (far below 1 kg/m^3) too low compared to those required to attain a significant contribution of

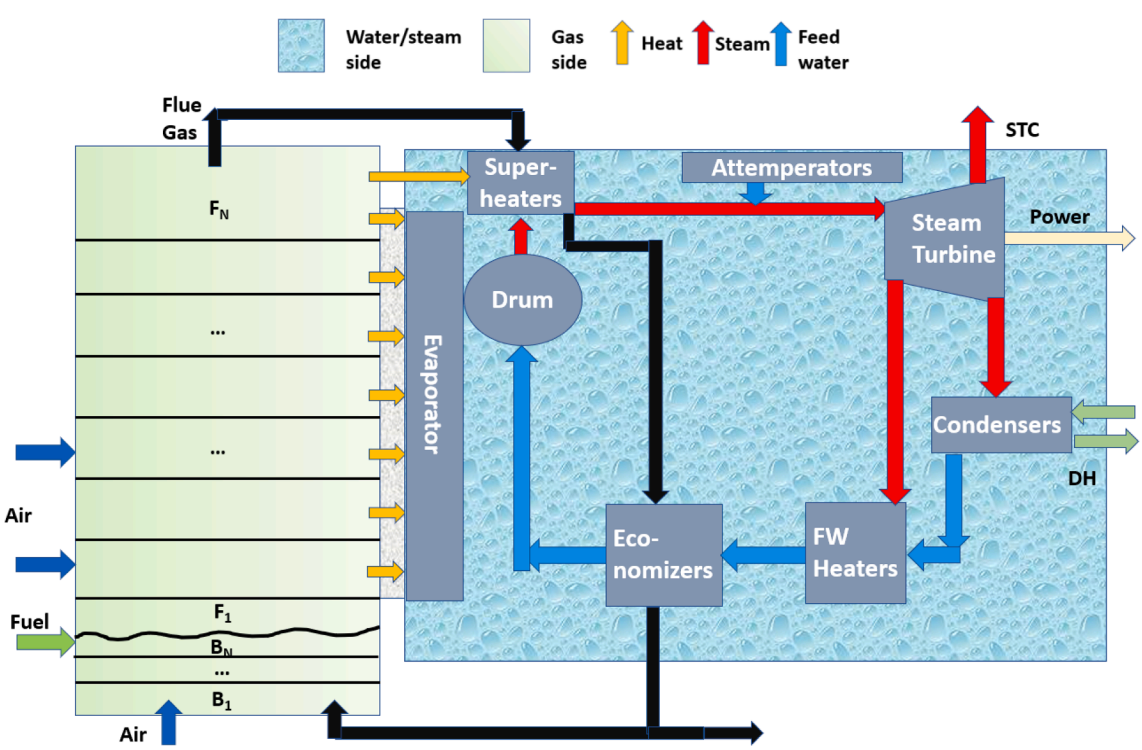

Fig. 4. Schematic of the dynamic plant model after integration of the gas side and water-steam side models. Discretization of the gas side is noted with B_i for the bed region and F_i for the freeboard.

Table 5
Modeled fuel (wood chips) analyses.

Proximate analysis, wt%	
Moisture	40.00
Volatiles	47.00
Char	12.60
Ash	0.40
Ultimate analysis (dry, ash-free), wt%	
C	50.60
H	5.90
O	43.20
N	0.08
S	0.04
HHV (dry, ash-free), MJ/kg	17.9

Table 6
Summary of the water-steam side model formulation.

Process equipment	Modeling approach	Correlations/equations
Monophasic flow tube heat exchangers (economizers and superheaters)	1-D lumped pipes separated from each other by a wall model	Nusselt based correlation for both sides [25].
Biphasic flow tube heat exchanger (evaporator)	1-D lumped pipes separated from the combustor side by a wall model	Nusselt correlation based on the Dittus-Boelter equation [26].
Steam drum	0-D for the liquid/vapor volumes. Heat transfer through the drum wall is neglected.	Formulations derived by Åstrom and Bell [27] and Eborn [24].
Steam turbine	Quasi-static assumption and isentropic efficiency constant with load	Stodolás Law of cones
Condensers / closed feedwater heaters	0-D for the liquid/vapor volumes and 1-D lumped pipes. A wall model separates them.	Correlation for condensing steam over horizontal tubes and Nu-based for the cold-fluid [25].
Open feedwater heater	0-D for the liquid/vapor volumes assuming thermodynamic equilibrium.	–
Spray attemperators	0-D mixing volumes	–
Valves	Linear valve opening flow. Flow assumed to be turbulent.	Flow computed from valve flow coefficient based on valve nominal conditions.
Pumps	Centrifugal pumps with constant rotational speed.	Quadratic flow characteristic.
Walls	1-D flat domain with heat accumulation.	Energy balance using a thermal resistance function of the thickness, area and conductivity.

convection to the bed-wall heat transfer. In this sense, industrial boiler measurements show that solids concentrations in the order of 10^0 kg/m^3 (i.e., above those found under bubbling conditions) yield a convective heat transfer to the walls of about 15–30 W/m^{2}K, compared to the total heat transfer of 100–200 W/m^{2}K [19]. The model includes a description of the radiative heat flows between all the surfaces and gas volumes accounting for geometrical view factors. Although the model neglects solids entrainment, it is well-known that the presence – even at very low concentrations not measurable by pressure transducers – of fine solids in the freeboard influences the effective emissivity of the gas. Therefore, the model computes the emissivity of volumetric cells (*vol*) according to Beeŕs Law, as shown in Equation (3), where the attenuation factor k_{vol} is a calibration factor that is dependent upon the gas velocity and L_p is the optical path length.

$$\varepsilon_{vol} = 1 - e^{-k_{vol}Lp} \tag{3}$$

The modeled fuel consists of wood chips, for which the proximate and ultimate analyses are shown in Table 5. In the model, fuel drying and devolatilization processes are assumed to be driven by heat transfer and to occur simultaneously, with a combined drying and devolatilization time that is dependent upon the fuel particle size taken from [20]. Char combustion is modeled through the shrinking sphere regime under transport-controlled conditions, while the combustion of gas species is computed using the rates described elsewhere [21]. The gas mixing in the freeboard is handled by the model as a calibration factor, through the tuning of the effective reaction rate of the homogeneous reactions (for details, see [8]).

The gas model was validated previously [8] using data from the reference BFB combustor. The validation showed that the model is capable of describing the in-furnace variables (such as temperatures and heat transfer to the waterwalls) with deviations of<10 % for the operational conditions considered for both the steady-state and transient operations. The reader is referred to [8] for a comprehensive description of the model formulation, calibration and validation.

4.2. Water-steam side

The water-steam model presented in this work has been developed following the model formulations for steam cycles presented in [22] and [23]. A summary of the followed approach and the principles underlying the main expressions used to model the different process components is shown in Table 6, while the specific correlations and equations can be found in Table A1. The water-steam side is calibrated through the tuning of a pre-exponential factor in the correlations for heat transfer coefficients, which is a common practice for dynamic process modeling [24]. Furthermore, the components modeled in 1-D are discretized into *N* elements, which is chosen as a compromise between model accuracy and computational cost. In addition, the model is initialized using the reference dataset of Load 1 (see Table 2).

The model includes the regulatory and supervisory control layers present in the reference plant. The former is devoted to maintaining the stability of the components, i.e., loops controlling levels, pressures, and temperatures in specific process units, while the latter is responsible for the production performance of the plant, i.e., controllers working on a minute-hour timescale. Among the different supervisory control strategies available for FBC-CHP plants (see [28] for a comprehensive review) this work includes a sliding-pressure structure, in which the combustion load Q_{comb} is used to control the plant output while the live steam pressure is controlled (but not fixed). Both layers are modeled as PI controllers and tuned according to the PID tuning rules of Skogestad [29].

5. Results and discussion

5.1. Validation of the model

The dynamic model presented in this work is validated against operational data obtained from the reference plant described in Section 2.1. The output of the model is validated both with steady-state and transient operational data, as a way to evaluate the capabilities of the model to describe typical operation of industrial-scale plants.

The BFB-CHP plant model is calibrated (as explained in Section 3.1) to resemble the design load (i.e., 100 % combustor load), represented by Load level 1 (see Table 2). After calibration, the output of the model at partial load is validated through simulation of Load level 2. Table 7 shows the comparison of the simulated process variables with the values measured in the industrial facility, as well as the absolute percentage error (AP; see Equation (4)) between them.

$$AP = 100\frac{|x_m - x_s|}{x_m} \tag{4}$$

It is clear that the model can reproduce multi-load, steady-state operation with a reasonable level of agreement, as all deviations are < 10 % with an average AP of 2.03 % (0.89 % and 3.17 % for the

Table 7
Results of the steady-state model validation.

Variable	Load level 1 (calibration)			Load level 2 (validation)		
	Measured	Simulated	AP (%)	Measured	Simulated	AP (%)
Live steam flow [kg/s]	53.4	54.3	1.7	29.5	29.6	1.0
Drum pressure [bar]	145	144	0.7	135	134	0.7
Live steam temperature [C]	540	540	0.0	540	540	0.0
Power production [MW]	36.0	35.5	1.4	16.5	17.8	7.9
DH production [MW]	49.2	49.4	0.4	31.8	30.1	5.3
DH outlet temperature [C]	105	104	1.0	82.5	85.9	4.1

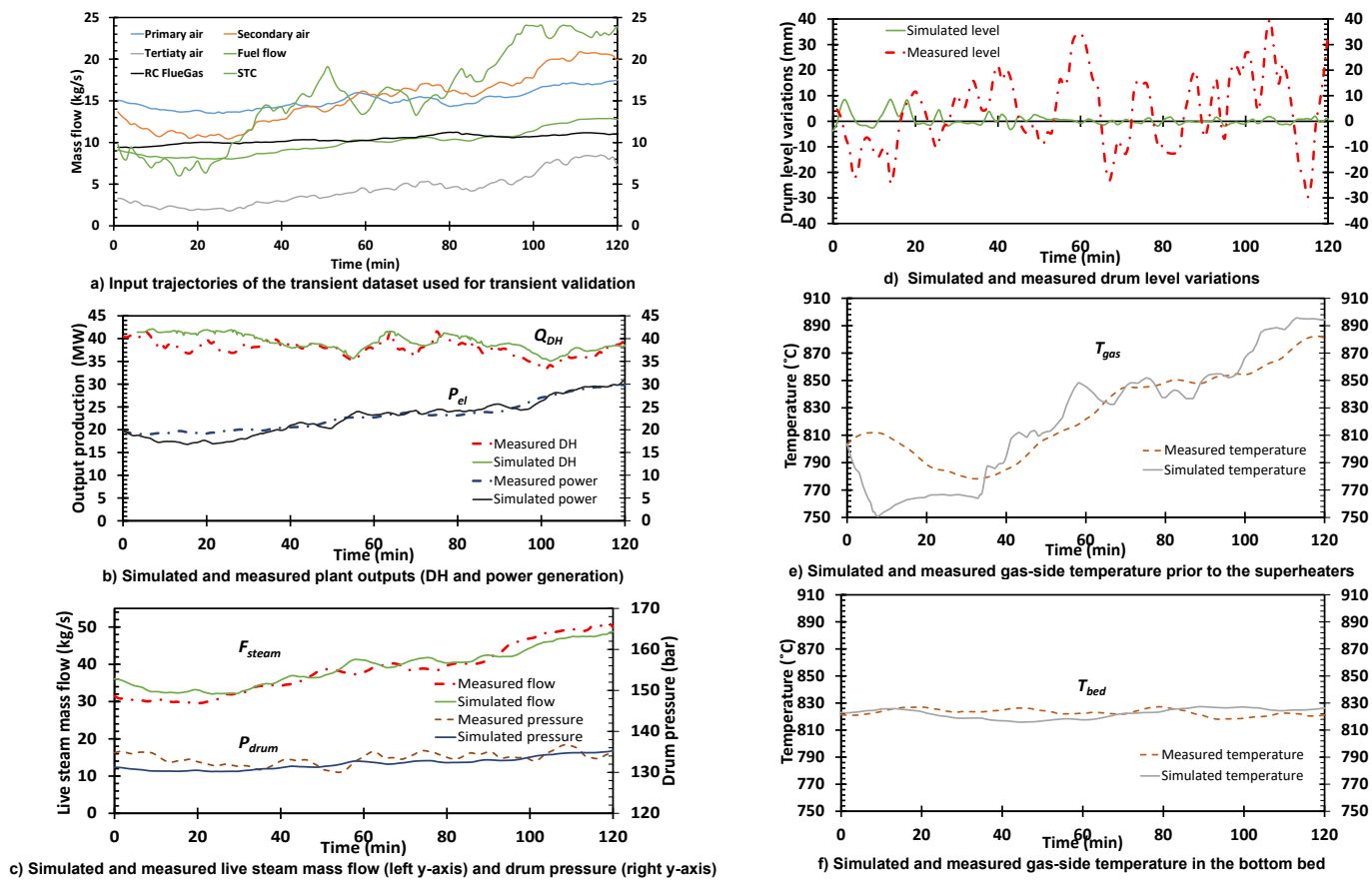

Fig. 5. Transient validation of the main plant model output variables. The figure includes: a) the input trajectories introduced into the model from measurements made in the reference plant; and b-f) a comparison of the simulated and measured variables of interest during the 120 min simulated.

calibration and validation cases, respectively). The observed deviations are within the same order as those observed in the validation of the gas side model. As discussed previously [8], the deviations can most likely be attributed to the fact that most of the semi-empirical expressions used in the model formulation of both sides were derived from data sampled at full-load operation.

To evaluate the capability of the model to describe transient operation, a 2 h-long dataset is used (which was also used in for validation of the gas side model, see [8]). This dataset covers a boiler fuel load increase from 56 % to 90 % and is simulated with the input trajectories of fuel, air, flue gas and STC mass flows, as shown in Fig. 5a. The output management strategy followed in the reference plant during the load change consisted of increasing the amount of steam delivered to customers while maintaining the DH production rather constant. This was achieved using the valve located between the high-pressure and low-pressure steam turbine sections (see Fig. 3).

Figure 5b-5f show the measured and simulated time trajectories of the main plant model variables, i.e., power and DH generation, steam mass flow, drum pressure and level as well as temperatures within the gas side. In general, the model is found to predict satisfactorily the behaviors of the reference plant across the 120 min simulated. Note that the model shows greater discrepancy with the measurements only within the first 20 min of the transient operation, which is the period during which the fuel flow and STC production are temporarily decreased (see inputs in Fig. 5a). With the inertia of the equipment being well-captured in the model formulation, this reduced model performance is likely due to discrepancies in the parameters of the supervisory and regulatory control layers (whose data is not available to the authors and is thus set by tuning according to [29]), which can be seen in the controlled drum level displayed in Fig. 5d: the systematic tuning introduced in the model shows more stable results than the signal measured in the plant. An additional potential source of errors might be in the input data for the incoming DH flow (which in this work, has been back-calculated). However, when evaluating the level of model agreement over the whole time series, it can be concluded that the ability of the model to predict steady-state and transient industrial operations is valid for the purpose of the model.

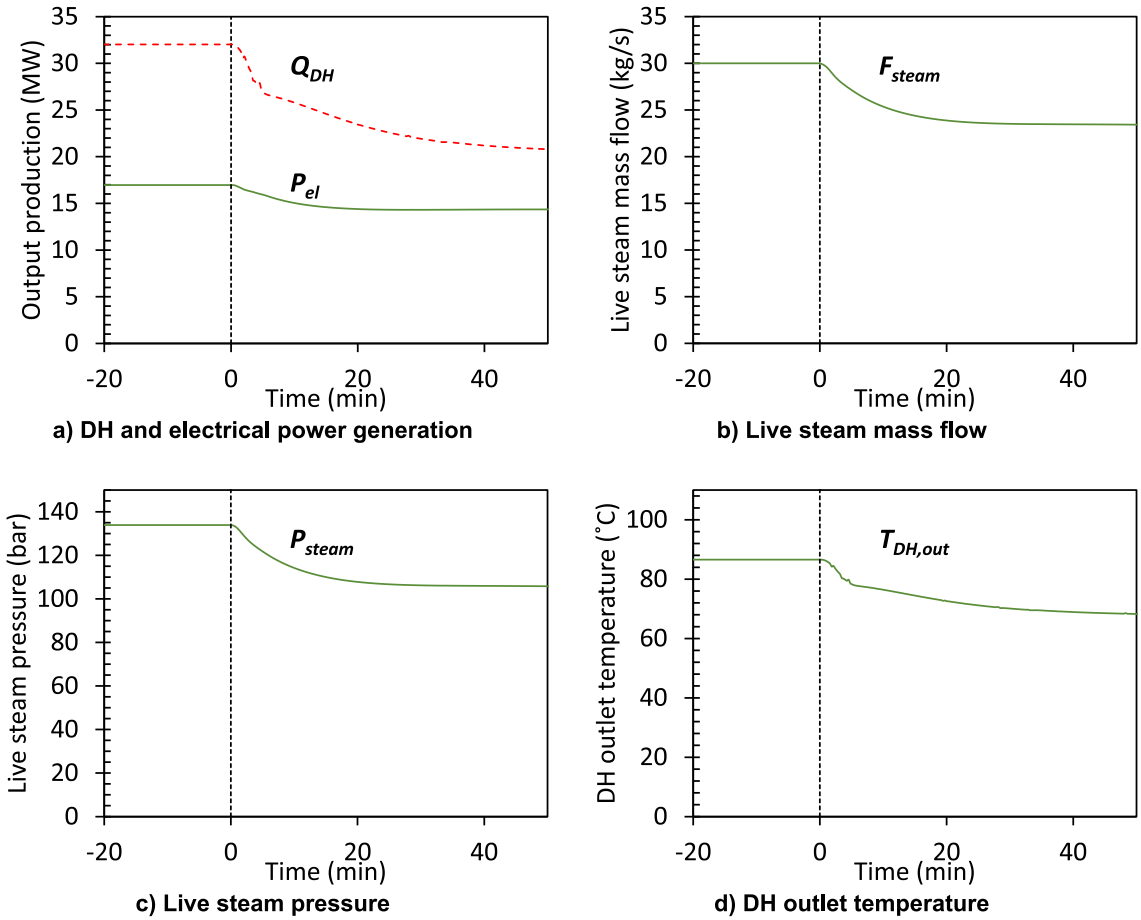

Fig. 6. Transient responses of the relevant process variables after a 20 % step change in the combustion load (see Table 3) is introduced at t = 0 (dashed vertical line).

5.2. Dynamic analysis

In order to illustrate the transient response of the plant after a step change is introduced, Fig. 6 shows the simulated open-loop transients of the main process variables when Q_{comb} is reduced at t = 0. The stabilization times and relative changes obtained from all the open-loop tests (see Table 3) are displayed in Fig. 7. The stabilization times shown in Fig. 7a range from an average of 17 min for changes to the combustion load to 2 min for changes to the DH line and to the STC flow. These differences are partly explained by the fact that Q_{comb} has the strongest steady-state effect on the process, as evidenced by the *RC*s plotted in Fig. 7b. In addition, changes to Q_{comb} are firstly introduced in the gas side before being propagated to the water-steam side, which entails an inherent delay compared to changes to F_{STC} and F_{DH}, both of which are introduced directly in the water-steam side, where the process dynamics are measured. The computed timescales and trends are in line with previous results obtained for FBC-CHP plants of similar size and layout as the one used here (see [28] for a dynamic analysis of a CFB-CHP plant, and [23] for an investigation that only includes the water-steam side of a waste-fired CFB). Furthermore, the data in Fig. 7b indicate that process variables connected to the DH production (i.e., Q_{DH} and $T_{DH,out}$) have the slowest stabilization times, in contrast to the variables connected to the live steam and steam turbine; this phenomenon was also identified in CFB-CHP plants assessed previously [23,28].

In Fig. 7b, it is important to note that changes in F_{STC} and F_{DH} barely affect the live steam conditions ($RC < 1$ %) and, therefore, the stabilization times for these cases have been disregarded in Fig. 6a. It is also noteworthy that a reduction in F_{STC} yields a slight reduction in the level of generated power. This is because, while the mass flow in the low-pressure stages of the turbine is increased (intuitively yielding an increase in generated power), the specific enthalpy drop across each turbine step does not remain constant (since the supervisory control loops are deactivated in the open-loop tests, which include the steam pressure control). This makes the intermedium pressures in the different turbine stages vary as the steam flow varies, thereby altering the pressures of the steam extractions and in the feedwater line.

For the reference BFB-CHP plant studied here, the characteristic times of the water-steam side can be compared to those of the in-furnace side reported earlier by the authors [8,9]. According to the previous study [8], while the temperatures at the bottom bed have characteristic stabilization times of 12 min, the stabilization times for the heat transfer to the waterwalls and the freeboard temperatures are in the range of 0.5–2.0 min for changes to Q_{comb} of similar size as those simulated herein. In [9], the authors explored the relationships between the stabilization times of key gas-side variables and the characteristic times of the three in-furnace mechanisms (namely, fluid dynamics, heat transfer and fuel conversion). The results showed that the stabilization times for the freeboard temperature and heat transferred to the waterwalls were largely driven by the fluid dynamics, i.e., the residence time of the gas, which for the BFB furnaces scoped in this work is in the order of 10–15 s. The results of the present work complete that picture by demonstrating that after changes are made to the combustion load, the stabilization of the water-steam side is governed by the large fluid and metal inventories (with the equipment connected to steam-only flows being faster). These results suggest that the water-steam side is an order of magnitude slower than the gas side in BFB combustion plants. i.e., being the eventual bottleneck for fast transient operation of biomass-fired BFB-CHP units.

The inherent transient response of the plant after changes in Q_{comb}

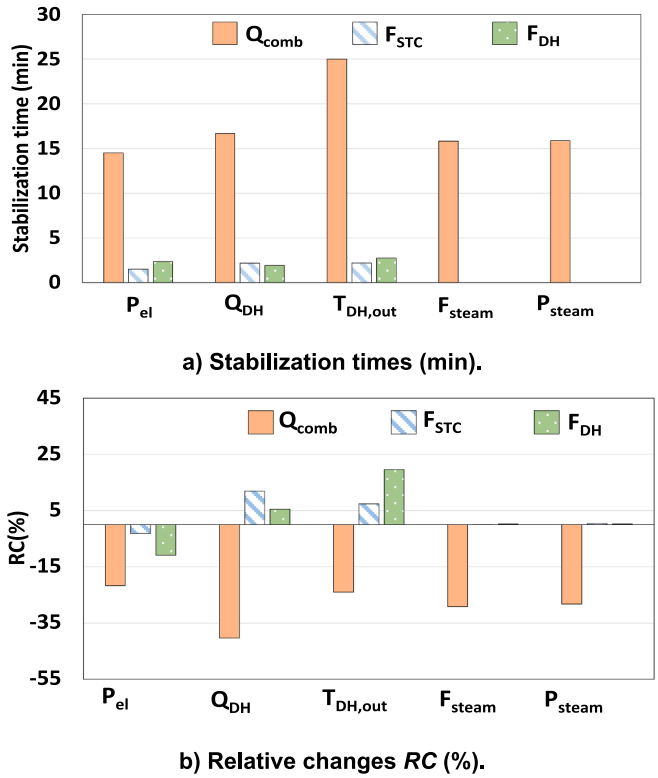

Fig. 7. Results from the open loop tests showing the impact on five main process variables as the input parameters are changed (see Table 3). Output variables: P_{el}, generated electricity; Q_{DH}, generated DH; $T_{DH,out}$, outlet DH temperature; F_{steam}, live steam mass flow; P_{steam}, live steam pressure. Input variables: Q_{comb}, combustion load; F_{STC}, mass flow of steam to customers; F_{DH}, DH mass flow.

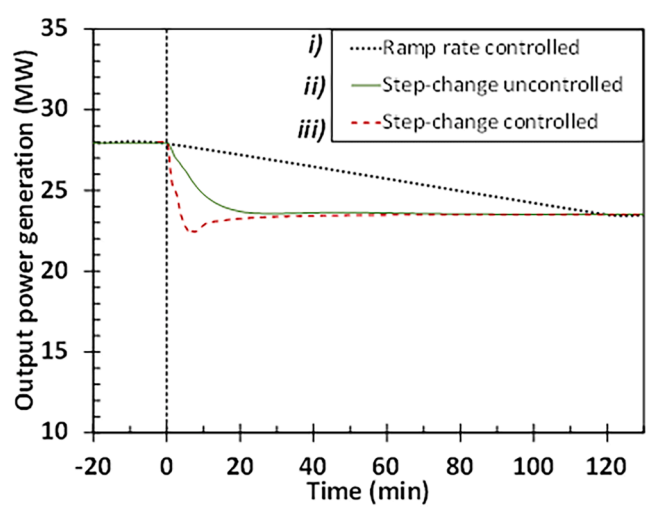

Fig. 8. Simulated output power generation when a 20 % change in the combustion load is introduced in t = 0 (represented with a dashed vertical line) as i) a current ramping rate as measured in the reference plant, ii) a step-change without supervisory control and iii) a step-change with supervisory control in place.

(which represents the main plant input to manipulate for changing the output load, see [28]) can be compared with that of the current plant operation. This is done in Fig. 8, which shows the output power generation, P_{el}, when Q_{comb} is decreased 20 % according to i) the current ramping rate of the reference plant, estimated from the dataset used for validation ii) a step-change with the plant in open-loop (displayed in Fig. 6a) and iii) a step-change with the plant under a conventional sliding-pressure supervisory control loop [28]. The controlled plant overperforms the inherent response by yielding a stabilization time for the power output < 10 min, in contrast to the 15 min for the latter and 120 min characterizing the current plant rate, which shows the potential of BFB-CHP plants for faster operation. Nonetheless, the eventual plant capability for flexible operation has to consider additional aspects such as the lifetime of technical components and other economic metrics [30].

6. Conclusions

This work presents a dynamic model of BFB-CHP plants that includes both the gas (in-furnace) side and the water-steam side as well as the control structures that regulate the plant operation. The plant model is validated with operational data from an industrial reference unit and is subsequently used to compute the inherent (open-loop) dynamic behaviors of the main process variables under transient operation. It has been found that the dynamic model presented herein can satisfactorily describe the steady-state and transient operations of large-scale BFBC plants within the load range that is typical for these units (i.e., 50–100 %).

Based on the results presented and discussed, the following conclusions regarding the dynamics of large-scale BFBC plants can be drawn:

- The computed stabilization times of all the process variables remain under 25 min for the cases investigated, with changes introduced in the combustor being those that have the strongest impact and yield the longest stabilization times.
- In general, the generated power stabilizes faster than the DH production.
- When comparing the results presented here with those of previous investigations of the dynamics of the gas side carried out by the authors, the dynamics of the water-steam side is found to be an order of magnitude slower than that the gas side. Thus, with the water-steam side governing the dynamics, these results suggest that CHP plants with a BFB furnace have similar transient plant abilities than CHP plants with other furnace technologies with faster response (e.g., pulverized fuel burners).

The results obtained and conclusions drawn in this work represent relevant information when assessing the transient operation capabilities of large-scale, biomass-fired BFB plants. Moreover, pertinent modeling assumptions can be derived from the findings of the present work when it comes to representing the timescales of the gas and water-steam sides. Nonetheless, further investigations including techno-economic considerations related to flexible operation such as thermal stresses, as well as control and operational strategies are required to better understand the dynamic capabilities of large-scale BFBC plants.

Declaration of Competing Interest

The authors declare that they have no known competing financial interests or personal relationships that could have appeared to influence the work reported in this paper.

Data availability

The authors do not have permission to share data.

Acknowledgments

The authors express their gratitude for the financial support provided by the Swedish Energy Agency (project 46459-1, “Cost-effective and flexible polygeneration units for maximised plant use”).

Appendix A. . Water-steam side model

Table A1 complements Section 3.2 by including a more detailed description of the model formulation of the water-steam side.

Table A1
Equations used to model the different components of the water-steam side model.

Process equipment	Formulation/magnitude	Correlation/Equation	Ref
Economizers and Superheaters	Heat transfer gas side	$\alpha = C\frac{F_a Nu_0 \lambda}{d_{hyd}}$	[25]
	Energy balance gas side	$\dot{m}(h_{out} - h_{in}) = \alpha A(T_{gas} - T_{wall})$	–
	Mass balance gas side	$\frac{d\dot{m}}{dt} = 0$	[31]
	Heat transfer water/steam side	$\alpha = C\frac{Nu_0 \lambda}{d_{hyd}}$	[25]
	Mass balance water/steam side	$\frac{d\dot{m}}{dt} = \dot{m}_{out} - \dot{m}_{in}$	–
	Pressure drops	$dp = \frac{K_f \dot{m}^2}{\rho}$ $K_f = \frac{dp_{nom} * LF * \rho_{nom}}{\left(\frac{\dot{m}_{nom}}{n_{channels}}\right)^2}$	[23,32]
Evaporator tubes	Heat transfer water side	$\alpha_{tp} = \psi \alpha_{Liq}$ $\psi = f(Co, Bo)$ $\alpha_{Liq} = 0.023 Re^{0.8} Pr_{Liq}{}^{0.4} (\frac{\lambda_{Liq}}{d_{hyd}})$ $Co = \left[\frac{1-x}{x}\right]^{0.8} \left[\frac{\rho_v}{\rho_{Liq}}\right]^{0.8}$ $Bo = \frac{q}{G \bullet h_{vap}}$	[33]
	Pressure drops	$dp = \frac{K_f \dot{m}^2}{\rho} = 0$ $K_f = \frac{dp_{nom} * LF * \rho_{nom}}{\left(\frac{\dot{m}_{nom}}{n_{channels}}\right)^2}$	[23,32]
Steam turbine	Stodola Law of cones for off-design conditions	$K_t = \frac{\dot{m}_n}{\sqrt{p_{i,n}\rho_{i,n}\left(1 - \left(\frac{p_{0,n}}{p_{i,n}}\right)^2\right)}}$	[34]
	Dry isentropic efficiency degradation	$\eta_{is,wet} = \eta_{is,dry} - \beta(1 - x)$	[35]
	Energy balance	$h_{out} = h_{in} - \eta_{is}(h_{in} - h_{is})$	–
	Generator	$P_{el} = \eta_{mech}\dot{m}(h_{in} - h_{out})$	–
Condensers / Closed feedwater heaters	Mass balance hot side	$\frac{d\dot{m}}{dt} = \dot{m}_{in} - \dot{m}_{out}$	–
	Heat transfer hot side	Correlation for film condensation over horizontal tube bundles $= f(Re, Pr, x, p, p_{crit}, d_{hyd})$	[25]
	Mass balance cold side	$\dot{m}_{in} = \dot{m}_{out}$	[23]
	Driving force heat transfer cold side	$\Delta T_{LM} = \frac{T_{wall} - T_{in}}{T_{wall} - T_{out}}$	[25]
Open feedwater heater	Energy balance	$\frac{dE}{dt} = \dot{m}_c h_c + \dot{m}_{st} h_s - \dot{m}_{fw} h_{fw}$	–
	Mass balance	$\frac{d\dot{m}}{dt} = \dot{m}_c + \dot{m}_{st} - \dot{m}_{fw}$	–
Valves	Linear valve characteristic	$\dot{m} = \theta \bullet C_v \bullet \frac{\dot{m}_{nom}}{\sqrt{\rho \bullet dp_{nom}}} \sqrt{\frac{p_{in} - p_{out}}{dp_{nom}}}$	[36]
Pumps	Volume flow rate	$\dot{V}_2 = \dot{V}_1 \left(\frac{N_2}{N_1}\right)\left(\frac{d_2}{d_1}\right)$	–
	Total head	$H_2 = H_1 \left(\frac{N_2}{N_1}\right)^2 \left(\frac{d_2}{d_1}\right)^2$	–
Walls (connecting sides of heat exchangers)	Heat accumulation	$\frac{m_{wall} c_p dT}{dt} = \frac{2(T_{wall,g} - T_{wall,steam/water})}{R_w}$	
	Heat resistance	$R_w = \frac{s/\lambda}{A}$	–

References

[1] Runge A, Metzger EC. A Clean Planet for all Vision for a Clean Planet by 2050. Eur Comm 2018;no. November:393.
[2] Commission E. Roadmap 2050. Policy 2012;no. April:1–9. https://doi.org/10.2833/10759.
[3] IEA, "Nuclear Power in a Clean Energy System," 2019.
[4] Scala F. Fluidized bed technologies for near-zero emission combustion and gasification. Cambridge: Woodhead Publishing Series; 2013.
[5] Kjärstad J, Johnsson F. The European power plant infrastructure-Presentation of the Chalmers energy infrastructure database with applications. Energy Policy 2007;35(7):3643–64. https://doi.org/10.1016/j.enpol.2006.12.032.
[6] Beiron J, Montañés RM, Normann F, Johnsson F. Combined heat and power operational modes for increased product flexibility in a waste incineration plant. "Combined heat and power operational modes for increased product flexibility in a waste incineration plant" 2020;202:117696.
[7] Wel M, McMillan CA, De la Rue Can S. Electrification of Industry: Potential, Challenges, and Outlook. Curr Sustain Energy Reports 2019;6(4):131–9. https://doi.org/10.1007/s40518-019-00143-2.
[8] Martinez Castilla G, Montañés RM, Pallares D, Johnsson F. Dynamic Modeling of the Reactive Side in Large-Scale Fluidized Bed Boilers. Ind Eng Chem Res 2021;60(10):3936–56. https://doi.org/10.1021/acs.iecr.0c06278.
[9] Castilla GM, Montañés RM, Pallarès D, Johnsson F. Comparison of the Transient Behaviors of Bubbling and Circulating Fluidized Bed Combustors. Heat Transfer Eng 2023;44(4):303–16.
[10] K. Atsonios, A. Nesiadis, N. Detsios, K. Koutita, N. Nikolopoulos, and P. Grammelis, "Review on dynamic process modeling of gasification based biorefineries and bio-based heat & power plants," *Fuel Process. Technol.*, vol. 197, no. March 2019, p. 106188, 2020, doi: 10.1016/j.fuproc.2019.106188.
[11] Selçuk N, Degirmenci E. Dynamic Simulation of Fluidized Bed Combustors and its Validation Against Measurements Dynamic Simulation of Fluidized Bed Combustors and its Validation Against Measurements. Combust Sci Technol 2001;167(December):1–27. https://doi.org/10.1080/00102200108952175.
[12] Yasar MS, Selçuk N, Kulah G. Performance and validation of a radiation model coupled with a transient bubbling fluidized bed combustion model. Int J Therm Sci 2022;176(1):107496. https://doi.org/10.1016/j.ijthermalsci.2022.107496.
[13] T. Kataja and Y. Majanne, "Dynamic Model of a Bubbling Fluidized Bed Boiler," in *14th Nordic Process Control Workshop*, pp. 140–149.
[14] Galgano A, Salatino P, Crescitelli S, Scala F, Maffettone PL. A model of the dynamics of a fluidized bed combustor burning biomass. Combust Flame 2005;140(4):371–84. https://doi.org/10.1016/j.combustflame.2004.12.006.
[15] M. Zlatkovikj, V. Zaccaria, I. Aslanidou, and K. Kyprianidis, "Simulation study for comparison of control structures for BFB biomass boiler," in *61st SIMS Conference on Simulation and Modelling*, 2020, no. September.
[16] Modelica Association, "Modelica and the Modelica Association," 1996. [Online]. Available: https://www.modelica.org/. [Accessed: 14-May-2021].
[17] Zhang Y, Li Q, Zhou H. Theory and calculation of heat transfer in furnaces. Elsevier; 2016.
[18] Vakkilainen E. Steam generation from biomass: Construction and design of large boilers. Elsevier; 2017.
[19] Breitholtz C, Leckner B, Baskakov AP. Wall average heat transfer in CFB boilers. Powder Technol 2001;120(1–2):41–8. https://doi.org/10.1016/S0032-5910(01)00345-X.
[20] S. Oka, *Fluidized bed combustion*. New York, 2004.
[21] Flagan RC, Seinfeld JH. Fundamentals of air pollution engineering. Englewood Cliffs, New Jersey: Prentice Hall; 1988.
[22] G. Martinez Castilla, "Dynamics of large-scale fluidized bed combustion plants," *Licent. thesis*, 2021, doi: https://research.chalmers.se/publication/524159.
[23] Beiron J, Montañés RM, Normann F, Johnsson F. Dynamic modeling for assessment of steam cycle operation in waste-fired combined heat and power plants Absolute Percentage Deviation. Energy Convers Manag 2019;vol. 198, no. August:111926. https://doi.org/10.1016/j.enconman.2019.111926.
[24] Eborn J. On model libraries for thermo-hydraulic applications. Dep Autom Control Lund Inst Technol 2001:135.
[25] Springer Ed. *VDI Wärmeatlas*, 9th Editio. Springer; 1997.
[26] Bhambare KS, Mitra SK, Gaitonde UN. Modeling of a coal-Fired Natural Circulation Boiler. J Energy Resour Technol Trans ASME 2007;129(2):159–67. https://doi.org/10.1115/1.2719209.
[27] Astrom J, K. and D. Bell, R.,. Drum-boiler dynamics. Automatica 2000;36:363–78.
[28] Martinez Castilla G, Montañés RM, Pallarès D, Johnsson F. Dynamics and control of large-scale fluidized bed plants for renewable heat and power generation. Appl Therm Eng 2023;219(119591):pp. https://doi.org/10.1016/j.applthermaleng.2022.119591.
[29] S. Skogestad, "Probably the best simple PID tuning rules in the world," in *AIChE Annual Meeting*, 2001, no. November 2001.
[30] Beiron J, Montañés RM, Normann F, Johnsson F. Flexible operation of a combined cycle cogeneration plant – A techno-economic assessment. Appl Energy 2020;vol. 278, no. August:115630. https://doi.org/10.1016/j.apenergy.2020.115630.
[31] Dechamps PJ. Modelling the transient behaviour of heat recovery steam generators. Proc Inst Mech Eng Part A J Power Energy 1995;209(4):265–73.
[32] Liu H, Hibiki T. Flow regime transition criteria for upward two-phase flow in vertical rod bundles. Int J Heat Mass Transf 2017;108:423–33. https://doi.org/10.1016/j.ijheatmasstransfer.2016.12.029.
[33] Modelon AB, "Modelon Home," 2018. [Online]. Available: https://www.modelon.com/.
[34] H. C. Cooke, "On prediction of off-design multistage turbine pressures by Stodolás Ellipse," *J.Eng. Gas Turbines Power*, vol. July, 107, no. 3, pp. 596–606, 1985.
[35] O. Bolland, *Thermal Power Generation*. 2014.
[36] M. B. Dzodzo, B. Liu, A. Cioncolini, and S. R. Spiegelman, "Application of CFD for Modeling Flows in Feed-Water Pipelines." pp. 293–301, 17-Jul-2006, doi: 10.1115/ICONE14-89549.